The pressure induced phase transition of confined water from *ab initio* molecular dynamics simulation

2004 J. Phys.: Condens. Matter 16 8851

(http://iopscience.iop.org/0953-8984/16/49/004)

INSTITUTE OF PHYSICS PUBLISHING JOURNAL OF PHYSICS: CONDENSED MATTER

J. Phys.: Condens. Matter **16** (2004) 8851–8859 PII: S0953-8984(04)76517-0

The pressure induced phase transition of confined water from *ab initio* molecular dynamics simulation

Sheng Meng[1,2], **E G Wang**[2] **and Shiwu Gao**[1]

[1] Department of Applied Physics, Chalmers University of Technology and Göteborg University, SE-412 96 Göteborg, Sweden
[2] Institute of Physics, Chinese Academy of Sciences, PO Box 603, Beijing 100080, People's Republic of China

Received 19 February 2004, in final form 4 October 2004
Published 26 November 2004
Online at stacks.iop.org/JPhysCM/16/8851
doi:10.1088/0953-8984/16/49/004

Abstract

We present an *ab initio* molecular dynamics study of pressure induced melting of an ice thin film confined between two parallel metal surfaces. The ice-to-water phase transition was observed at a pressure of roughly 0.5 GPa, when the film was compressed by 6.6%. The latter is in agreement with the volume change in the melting of bulk ice. The effects of nonadiabatic compression on the layer-dependent momentum distribution and the electronic redistribution at the interfaces are presented and discussed.
(Some figures in this article are in colour only in the electronic version)

1. Introduction

Water in a confined space (confined water) [1–3] exhibits unusual behaviours and properties that differ from those of its bulk counterpart. It is ubiquitous in natural materials such as Vycor glass [4] and in biological systems such as proteins [5] and biomembranes [6]. The microscopic behaviour of confined water determines the structure and functions of these systems through, for example, polar ordering [7, 8], intermolecular coupling, viscosity [9], dissipation [10], protein folding [5], and conformational transformations. The study of confined water has been a subject of intensive theoretical and experimental study, using in particular computer simulations. This paper studies the pressure induced phase transition of water confined between two parallel surfaces [11–13], a model system; the findings have implications for many dynamical processes such as lubrication, friction, skating, and premelting, where water in different confinement and pressure regimes affects the structure and behaviour of these systems.

Generally speaking, the confinement and compression of water lead to two different effects:

(i) reduced geometric space, which results in shortening of the hydrogen bonds (H bonds) between water molecules; and
(ii) the disruption and modification of the H bonds of the interface molecules.

Both effects depend on the atomic configurations of the confined water, and ultimately the electronic interactions between the constituent atoms. The latter should evolve with the macroscopic boundary conditions introduced by confinement and pressure. Therefore, a *self-consistent* description of the atomic interactions and geometric confinement is essential to the general understanding of confined water and its response to pressure. Previous simulations of confined water were all based on classical molecular dynamics (MD), with model potentials accounting for the inter-water interaction and water–surface interaction [14–17]. *Ab initio* description of the confinement and pressure has been a great challenge due to the very demanding computations required by *ab initio* electron structure calculation, although the density functional theory (DFT) has been successfully applied to water clusters [18], bulk ice and liquid water [19–21], and water at metal–water and semiconductor–water interfaces [22, 23].

Here, we report the first *ab initio* molecular dynamics study of the pressure induced melting of confined water based on a density functional description of atomic potentials. By placing a thin film of ice Ih between metal (Pt) slabs, pressure melting has been simulated by a gradual reduction of the film thickness. It has been found that melting of the ice occurs at a pressure of roughly 0.5 GPa, corresponding to a volume contraction of 6.6%. The latter is in agreement with the volume change in the solid–liquid transition of bulk ice. Further increase of pressure in the liquid region results in linear heating. The liquid phase is characterized by much more delocalized trajectories and the frequent breaking and recombination of hydrogen bonds. The confinement and compression lead to a layer-dependent kinetic energy distribution, which relaxes to equilibrium on a picosecond timescale in both solid and liquid phases. Substantial electronic redistribution involved in the confinement and compression at the interfaces has also been observed. The results demonstrate the feasibility and necessity of *ab initio* simulations for the description of confined water and related phenomena.

2. Simulation methods

The calculation has been performed using the Vienna *ab initio* simulation package, VASP [24, 25]. The supercell consists of a slab with four-layer Pt atoms in the (111) surface and a 4-bilayer of ice arranged in a $(2\sqrt{3} \times 2\sqrt{3})$R30° symmetry, which accommodates 32 water molecules between the Pt slabs (see the inset of figure 1). This bilayer geometry matches that of a Pt substrate on one side (bottom layer), whose initial atomic coordinates were obtained from the adsorption of water on this surface. The other side (the top layer) of the ice–Pt interface forms an incommensurate contact. Such an asymmetric model allows us to study interface water and confined water simultaneously and their dynamical responses to pressure under different boundary conditions. The energy cut-off for the plane waves is set to 300 eV. A single k-point sampling at $(1/2, 1/2, 0)$ is used for electron density generation, while the Fermi level is smeared by the Methfessel–Paxton method [26] with a Gaussian width of 0.4 eV. This set of parameters ensures a total energy convergence of 0.015 eV per atom. The Vanderbilt ultrasoft pseudopotentials (USPPs) [27] and the generalized gradient approximation (GGA) for the exchange–correlation energy given by Perdew and Wang (PW91) [28] are used throughout.

The pressure is applied by reducing the thickness of the supercell while keeping the Pt atoms fixed in the positions that they occupy in the bulk solid (with the calculated lattice constant 3.99 Å). This is feasible due to the very small vertical relaxation (less than 2%) for the free Pt(111) surface and the surface being under pressure up to several gigapascals. The compression of the film was simulated by varying the thickness of the supercell, ranging from the initial value of $z = 23.41$ Å ($\Delta z = 0$) to a minimum thickness of $z = 21.91$ Å ($\Delta z = -1.5$ Å). The water–Pt distances at the upper and lower interfaces were

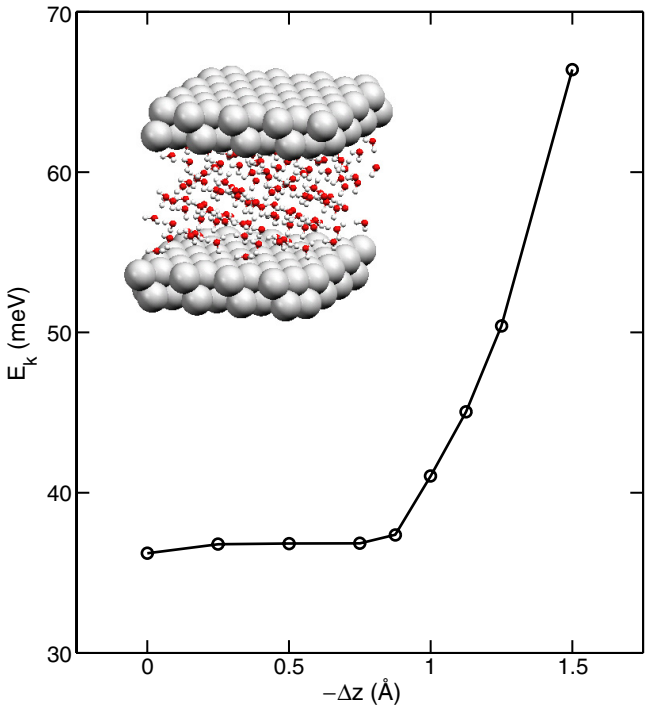

Figure 1. The calculated mean kinetic energy per atom versus the thickness change of the water film, Δz. These kinetic energies correspond to temperatures of 280, 284, 285, 285, 289, 317, 348, 375, and 513 K, respectively, for the simulated slabs. The inset shows schematically the atomistic model of the simulation.

reduced equally during compression. Each simulation at a given slab thickness was carried out with fixed wall separation. At each slab thickness z, the system was first equilibrated for typically 0.5 ps (with a time step of 0.5 fs, as in our previous study [29]), starting from the same initial positions and velocities as at $\Delta z = 0$. An additional 1–2 ps molecular dynamics run in constant energy mode was performed to record the trajectories for analysis. These timescales were found to be enough for analysing the properties of the total system, but seem to be short for equilibration between the different bilayers of the ice film. To further study the effect of the nonadiabatic compression, longer MD runs were carried out for the compressed films. Equilibration between the layers was achieved at about 3–5 ps.

3. Results and discussion

3.1. The pressure induced ice–water phase transition

Figure 1 shows the total kinetic energy of the water film versus the change in its thickness, Δz, as it is compressed in the normal direction. These kinetic energies are averaged over 0.5–1 ps trajectories in the MD runs. Obviously, this curve can be divided into two regions: (i) a flat region between $\Delta z = 0$ and -0.875 Å; and (ii) an almost linear region from $\Delta z = -0.875$ to -1.5 Å. The flat region indicates that the potential (internal) energy of the ice does not change appreciably when the ice film is compressed at the initial stage. This results from the rather flat potential of bulk ice [30] near the equilibrium volume. It is also the microscopic origin of

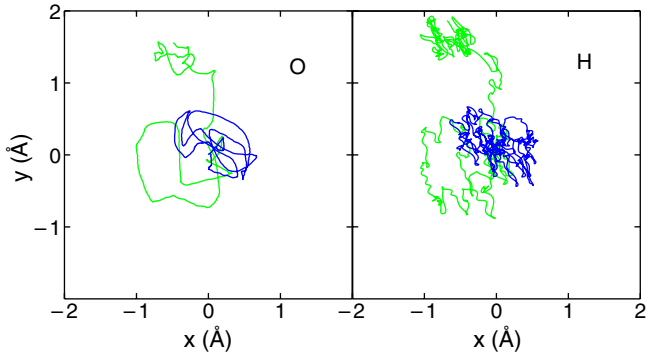

Figure 2. Typical molecular trajectories projected in the xy plane before (black curve) and after the phase transition (grey curve), taken at $\Delta z = -0.75$ and -1 Å, respectively. The trajectories are for an O atom (left panel) and an H atom (right panel) in the same molecule during a 1.8 ps MD run.

the latent heat, which is generally observable in water and other solid–liquid phase transitions. The flat region can be assigned to solid ice. Further compression of the ice, $\Delta z > -0.875$ Å, leads to rapid increase in the kinetic energy and a simultaneous increase in the potential energy (not shown), indicating the transfer of external work into internal energy of the water film. This rapid increase of kinetic energy marks therefore the formation of liquid water. The sudden increase at $\Delta z = -0.875$ Å suggests a first-order solid–liquid phase transition. The thickness at the melting point corresponds to a volume change in the ice film of 6.6%, which compares well with the experimental value of 6.4% when ice melts [31]. The compression, which leads to shortening of the hydrogen bonds and the energy transfer, is responsible for the ice melting taking place in figure 1. By averaging the forces on the surface atoms during the MD runs, the pressure imposed on the Pt surface has been evaluated, which provides a calibration of the pressure applied on the water film. Roughly, $\Delta z = -1$ Å corresponds to a pressure of 0.5 GPa.

3.2. Dynamics of water molecules around the phase transition

The phase transition in the thin film can be alternatively monitored from the atomic trajectories in the MD runs. Figure 2 shows typical trajectories for the O (left panel) and H (right panel) atoms in a water molecule before (black curve) and after (grey curve) the phase transition. These trajectories are sampled at $\Delta z = -0.75$ and -1 Å, respectively, and are projected into the xy plane for a 1.8 ps duration. After the phase transition, the trajectories are highly delocalized in the liquid water. The 2D phase space of liquid water is roughly 2–3 times larger compared to that of the ice. The self-diffusion coefficients, estimated from the slope of the mean square displacement of oxygen atoms, are <0.008 Å^2 ps^{-1} before melting ($\Delta z = -0.5$ Å) and 0.5 Å^2 ps^{-1} at $\Delta z = -1$ Å, when the ice just melts. The latter is comparable to the diffusion coefficient of liquid water at 300 K, 0.24 Å^2 ps^{-1} [20]. In addition, frequent rotational and librational motions can also be seen in figure 2 by correlating the trajectories of H and O atoms in the two panels, which shows that such motions are much more active in the liquid water. Layer-resolved trajectories indicate that the atoms in the bottom layer are much more localized than those in the central layers (not shown), suggesting a layering effect of confined water at the interface. A similar layering effect was also observed in a recent *ab initio* MD simulation at the Ag–water interface [22]. Other features of liquid water, such as the frequent breaking of H bonds and formation of new H bonds, have also been observed. Two such events are depicted in figure 3, where one of the H bonds was temporarily broken but soon reformed

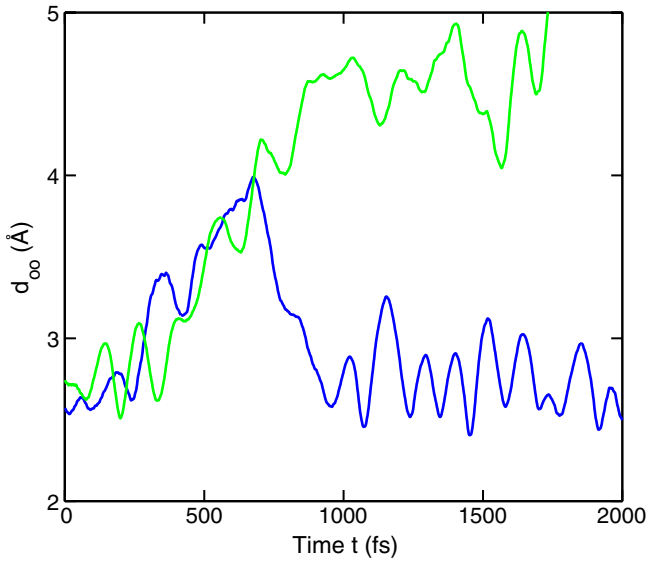

Figure 3. Hydrogen bond breaking and recombination dynamics from an MD simulation at $\Delta z = -1$ Å. One H bond (black curve) breaks temporarily and reforms, while the other H bond (grey curve) is simply broken.

(the black curve), while the other one simply broke (the dashed curve). The atomic trajectories and the self-diffusion coefficients confirm once again that a phase transition occurred in the film.

In order to quantify the structural transformation of the water film under compression, the pair correlation functions (PCF) of the atomic distribution for the two middle bilayers, averaged from MD trajectories, have been calculated and are shown in figure 4. The three panels show the atom-resolved PCFs as a function of the O–O (upper panel), O–H (middle panel), and H–H (bottom panel) distances at $\Delta z = 0$, -1, and -1.5 Å, respectively. Such functions are available for the bulk, but they are not straightforward for confined systems due to, for instance, excluded volume effects [32]. To avoid controversy, only atoms in the two middle bilayers, which resemble bulk, are chosen for analysis in our case. The black solid curves in figure 4 at $\Delta z = 0$, are very close to the PCFs for bulk ice with sharp peaks corresponding to the mean bond lengths in ice Ih. Upon compression, i.e. going from $\Delta z = 0$ to -1.5 Å, all the PCF peaks broaden and shift gradually, indicating softening of the H bond and delocalization of atomic motions as shown by the trajectories. This evolution is most pronounced for the second peak in $g_{OO}(r)$ at $r = 4.8$ Å, which is characteristic for the tetrahedral coordination in solid ice Ih. This peak gradually shifts downward and eventually loses its feature at $\Delta z = -1.5$ Å, when liquid water is formed. $g_{OO}(r)$ evolves into a rather flat distribution beyond the first peak. Such a uniform distribution at large distances is a characteristic feature for hydrogen bond dynamics in the liquid water, where the directional H bonding and coordination disappears. The PCF curves in figure 4 can be compared with neutron scattering data for bulk [33] and confined water [32]. The overall features, namely the peak positions and the widths, compare quite well, although the nearest O–O distance in the upper panel (2.7 Å) is about 6% shorter than the experimental value (2.87 Å). This minor discrepancy might result from the usually shorter hydrogen bond length predicted by the USPP-PW91 approach [29]. Furthermore, the modifications of PCFs from confinement are in good qualitative agreement with the experiment [32] and the previous simulation based on a classic water model [34]. For instance, the first peak of $g_{OO}(r)$ becomes less intense and the first minimum becomes shallower and is left-shifted upon confinement.

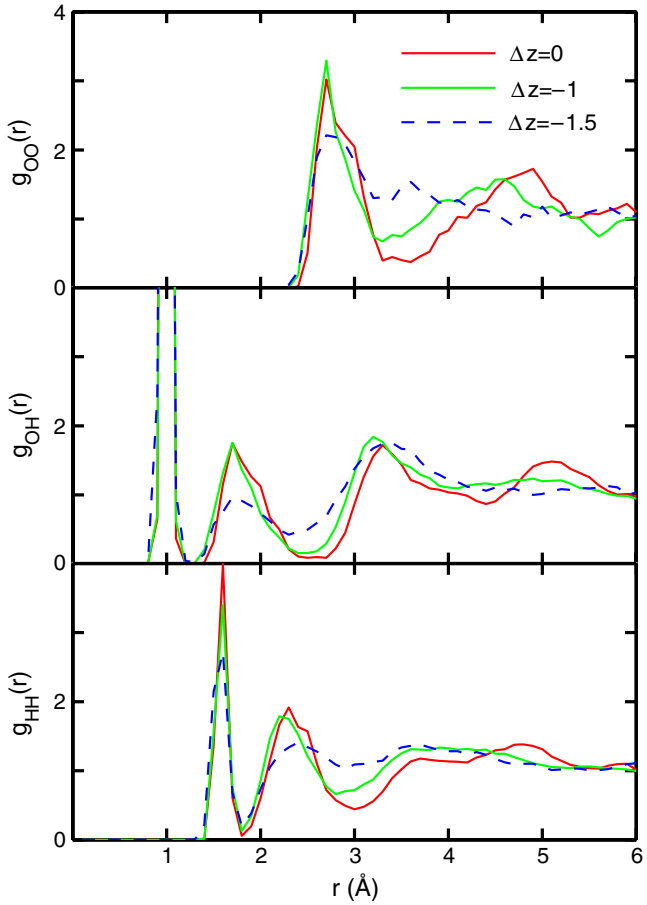

Figure 4. The pair correlation functions (PCF) for OO, OH, and HH pairs extracted from the MD simulations. The black, grey, and dashed curves were obtained at $\Delta z = 0$, -1, and -1.5 Å, respectively.

3.3. Effects of confinement and nonadiabatic compression

We now turn to discussing the effect of nonadiabatic compression on the layer-resolved quantities and the change of electronic states under phase transition. These issues are relevant because a sudden compression generates a large vertical force on the outer layers of the film. Initially the energy distribution between inner and outer layers is not equilibrated, and persists for a period of time before it reaches equilibrium. Our concern is how the re-equilibration takes place in the confined and compressed water film. This question is mainly technical, because it tells us whether the system is in equilibrium or not in a given duration of MD simulation. It is also in part physical, because it helps us to judge the nonadiabaticity of the compression process.

Figure 5 shows the layer-resolved kinetic energy distribution created by compressing the film from the initial equilibrium state by 1.0 Å. Both the parallel components in the xy plane (E_{kxy}) and the vertical component in the z direction (E_{kz}) were plotted for 3 ps. The vertical kinetic energy of the bottom layer (first layer) exhibits a dramatic initial increase, due to the fact that compression creates a larger vertical force in the bottom layer. (In some other cases,

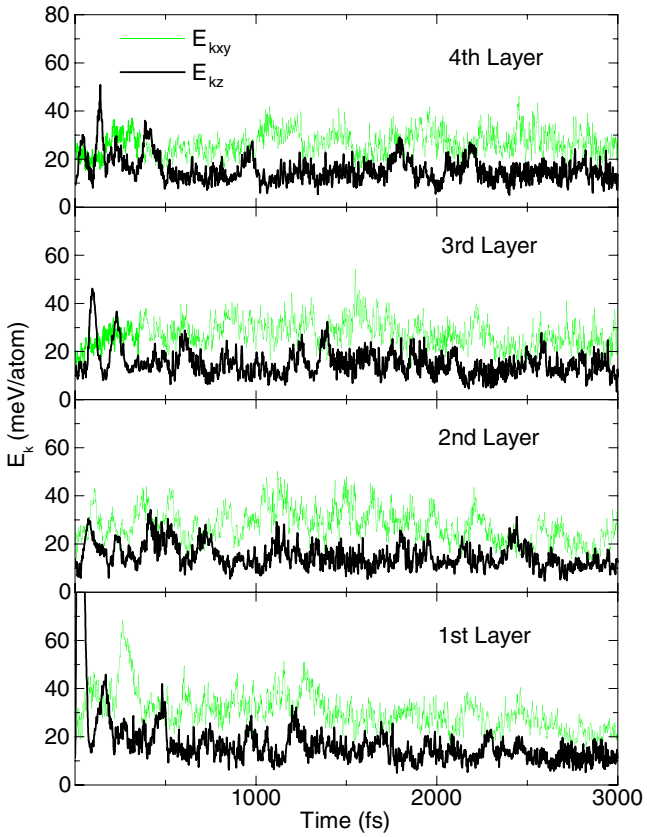

Figure 5. Relaxation of layer-resolved kinetic energy distributions, created by compressing the film by 1 Å. Both the parallel and perpendicular components are shown, for comparison.

such increase can be seen in both the bottom and top layers initially.) The kinetic energies of the other layers are less affected. The kinetic energy is then transferred primarily to the parallel components of the bottom layer. After 2–3 ps the kinetic energies in all layers relax to equilibrium again, with E_{kxy} and E_{kz} approaching about 24 and 12 meV, respectively. Similar layer-resolved studies were done for other states during the phase transition. While the details of the layer-resolved kinetic energies vary from case to case, the results are qualitatively the same: nonadiabatic compression leads to initial nonequilibrium distributions, which relax to equilibrium in 2–3 ps. It is interesting to note that similar behaviour was observed in previous MD simulations of pressure melting of small ice clusters, [35] where the melting was found to proceed from outer layers to inner ones consecutively. As the relaxation time, 2 ps, is much shorter than any mechanical timescale involved in applying pressure to a system, we can therefore conclude that the pressure induced phase transition of ice film is basically an equilibrium process.

Finally, we demonstrate the effect of confinement and compression on the electronic structure of the confined water. This information is only available in *ab initio* simulations, such as those we performed here. Figure 6 shows the one-dimensional (1D) charge density redistribution along the z direction. The 1D redistribution is defined by the density difference between the charge density of the total system (the Pt and the water film) and those of the separate Pt and water film in the same geometrical configurations. The three curves show

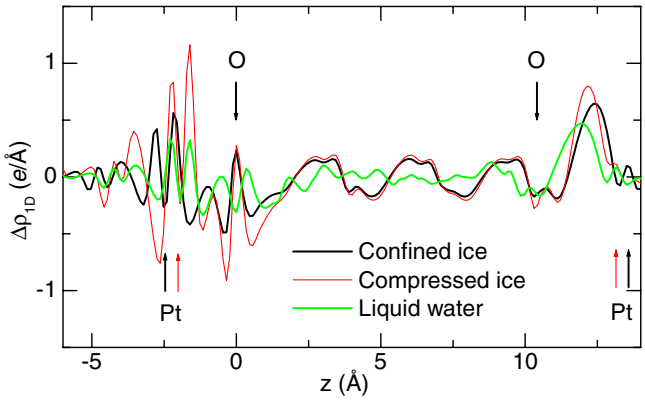

Figure 6. The one-dimensional electron density variation for the confined ice film at $\Delta z = 0$ (heavy black curve), the ice film compressed by $\Delta z = -1.0$ Å (thin black curve), and the melted water film (grey curve). The difference density is defined as the difference between the charge densities of the total system and those of the subsystems, i.e. the separate Pt and ice film at the same geometrical configurations. Arrows indicate the positions of the Pt and O atoms in the interface region.

the density variation of the equilibrated ice film under confinement ($\Delta z = 0$ Å), the ice film compressed by $\Delta z = -1.0$ Å, and the liquid water state where the phase transition had occurred, which was obtained by 3 ps MD simulations. The confined ice shows the bonding character at the ice–Pt interface (left region) and electron polarization at the noncommensurate contact (right region). A d_{z^2}–p_z bonding feature is clearly seen in the Pt–O region with electron transfer going from oxygen to Pt. In contrast, the right interface does not show any bonding character. Instead, it exhibits an electron polarization toward the interface. Compressing the film by 1 Å led to a shift of the peak positions and a remarkable increase in the density variations at the bonding interface. The change in the central water layers is almost negligible. The charge redistribution at the interfaces is the driving force for inducing the ice–water phase transition. When the liquid water forms, the electron distribution becomes much more smooth, especially in the central layers of water. This smoothness of the electron redistribution is NOT associated with the atomic delocalization of liquid water. It reflects the bare change of electronic states in the liquid water. It is also interesting to note that the bonding character of the electronic structure at the interfaces does not change when the film goes from confined ice, to compressed ice, and finally to liquid water. This indicates that the geometric structure of the interface does not change appreciably during phase transition. In other words, the confined water behaves like 'supercooled water', in agreement with previous structural analysis from both theoretical [15, 22] and experimental [7, 36] studies. The electronic redistributions shown in figure 6 illustrate the roles of the electronic structure and charge transfer in the water–metal interaction under confinement, compression, and phase transitions. Such information explains the importance of the *ab initio* simulations.

4. Summary

Summarizing, we have performed an *ab initio* molecular dynamics study of pressure melting of an ice thin film and observed the solid–liquid phase transition. The dynamics of the phase transition has been characterized in detail via the H bond breaking and reformation, the phase space expansion, and the evolution of the pair correlation functions. Our *ab initio* simulation also found substantial electronic redistribution under confinement and pressure at the water–Pt

interface. This study, the first of its type, demonstrates the feasibility of *ab initio* molecular dynamics simulation of pressure, confinement, and related phenomena. The results have broad implications for molecular dynamics simulations of confined water and its phase properties.

Acknowledgments

This work was supported by the Swedish Research Council (VR) through grant VR 621-2001-2614 and partially supported by the Natural Science Foundation of China (60021403, 10134030) and MOST (G2000067103, 2002AA311151). The allocation of computer time at the High Performance Computing Centre at North (HPC2N) and the National Computer Centre (NSC) in Sweden is gratefully acknowledged.

References

[1] Teixeira J, Zanotti J M, Bellissent-Funel M C and Chen S H 1997 *Physica* B **234** 370
[2] Bellissent-Funel M C 2001 *J. Phys.: Condens. Matter* **13** 9165
[3] Levinger N E 2002 *Science* **298** 1722
[4] Bruni F, Ricci M A and Soper A K 1998 *J. Chem. Phys.* **109** 1478
[5] Kasemo B 1998 *Curr. Opin. Solid State Mater. Sci.* **3** 451
[6] Yang L and Huang H W 2002 *Science* **297** 1877
Gruner M S 2002 *Science* **297** 1817
[7] Du Q, Freysz E and Shen Y R 1994 *Science* **264** 826
[8] Su X C, Lianos L, Shen Y R and Somorjai G A 1998 *Phys. Rev. Lett.* **80** 1533
[9] Raviv U, Laurat P and Klein J 2001 *Nature* **413** 51
[10] Antognozzi M, Humphris A D L and Miles M J 2001 *Appl. Phys. Lett.* **78** 300
[11] Bergman R and Swenson J 2000 *Nature* **403** 283
[12] Koga K, Tanaka H and Zeng X C *Nature* **408** 564
[13] Zangi R and Mark A E 2003 *Phys. Rev. Lett.* **91** 025502
[14] Xia X and Berkowitz M L 1995 *Phys. Rev. Lett.* **74** 3193
[15] Gallo P, Rovere M and Spohr E 2000 *J. Chem. Phys.* **113** 11324
[16] Foster K, Raghavan K and Berkowitz M 1989 *Chem. Phys. Lett.* **162** 32
[17] Price D L and Halley J W 1995 *J. Chem. Phys.* **102** 6603
[18] Laasonen K, Parrinello M, Car R, Lee C and Vanderbilt D 1993 *Chem. Phys. Lett.* **207** 208
[19] Lee C Y, Vanderbilt D, Laasonen K, Car R and Parrinello M 1993 *Phys. Rev.* B **47** 4863
[20] Laasonen K, Sprik M, Parrinello M and Car R 1993 *J. Chem. Phys.* **99** 9080
[21] Pfrommer B G, Mauri F and Louie S G 2000 *J. Am. Chem. Soc.* **122** 123
[22] Izvekov S and Voth G A 2001 *J. Chem. Phys.* **115** 7196
[23] Gayathri N, Izvekov S and Voth G A 2002 *J. Chem. Phys.* **117** 872
[24] Kresse G and Hafner J 1993 *Phys. Rev.* B **47** 558
Kresse G and Hafner J 1994 *Phys. Rev.* B **49** 14251
[25] Kresse G and Furthmüller J 1996 *Comput. Mater. Sci.* **6** 15
Kresse G and Furthmüller J 1996 *Phys. Rev.* B **54** 11169
[26] Methfessel M and Paxton A T 1989 *Phys. Rev.* B **40** 3616
[27] Vanderbilt D 1990 *Phys. Rev.* B **41** 7892
[28] Perdew J P, Chevary J A, Vosko S H, Jackson K A, Pederson M R, Singh D J and Foilhais C 1992 *Phys. Rev.* B **46** 6671
[29] Meng S, Xu L F, Wang E G and Gao S W 2002 *Phys. Rev. Lett.* **89** 176104
[30] Hamann D R 1997 *Phys. Rev.* B **55** R10157
[31] Brill V R and Tippe A 1967 *Acta Crystallogr.* **23** 343
[32] Soper A K, Bruni F and Ricci M A 1998 *J. Chem. Phys.* **109** 1486
[33] Soper A K 1994 *J. Chem. Phys.* **101** 6888
[34] Gallo P, Ricci M A and Rovere M 2002 *J. Chem. Phys.* **116** 342
[35] Weber T A and Stillinger F H 1984 *J. Chem. Phys.* **80** 438
[36] Reedijk M F, Arsic J, Hollander F F A, de Vries S A and Vlieg E 2003 *Phys. Rev. Lett.* **90** 066103